Tuning material properties via disorder: From crystalline alloy to metallic glass

Alessandro Troglia [a], Victor Vollema [a], Silvia Cassanelli [b], Erik van Heumen [b], Jorik van de Groep [b], Anne de Visser [b], Roland Bliem [a,b,*]

[a] Advanced Research Center for Nanolithography, Science Park 106, 1098 XG, Amsterdam, Netherlands
[b] Van der Waals–Zeeman Institute, Institute of Physics, University of Amsterdam, Science Park 904, 1098 XH, Amsterdam, Netherlands

ARTICLE INFO

ABSTRACT

Pathways to tune the electronic, chemical, mechanical, and optical properties of solids without modifying their composition represent a new paradigm in the design of functional and sustainable materials. The level of structural disorder - from perfectly crystalline to fully amorphous – for example, induces remarkable changes in material properties. Typically, disorder is introduced by altering the composition of a material, adding to the misconception that these two properties cannot be decoupled. Here, we demonstrate that striking differences in the optical, electronic, and corrosion properties of CuZr are achieved by deliberately and reproducibly engineering the level of structural disorder in pulsed laser deposited thin films of a constant composition. This approach allows tuning the structure of CuZr from polycrystalline to fully amorphous, switching the nature of charge transport from metallic to semiconductor-like, the optical properties in the visible regime from opaque to transparent, and the corrosion behavior in air from mixed oxidation to the formation of a protective Zr oxide overlayer. Our results highlight the tunability of structural disorder in alloys and its remarkable effect on material properties, providing the opportunity to design sustainable functional materials based on customizing properties beyond their composition.

1. Introduction

Structural disorder in materials is intuitively often considered detrimental compared to the well-defined long-range order offered by crystalline solids. However, several examples of amorphous materials are known to exhibit superior properties to their crystalline counterparts. Metallic glasses [1–4], for example, have gained considerable attention due to their corrosion resistance [5,6], mechanical strength [7,8], wear resistance [9], and permeability for diffusion [10]. Excellent performance in catalysis has also been reported for other amorphous materials [11,12]. The complete lack of long-range order at the atomic scale has been found to yield very different mechanical, optical and magnetic properties compared to crystalline materials [13–15]. In specific applications, the properties of amorphous solids already find appreciation in the thin-film regime, for example in microelectronic and biomedical devices and sensors [16,17]. The penetration of amorphous materials into new technological fields of application is, however, partly limited by the perceived lack of flexibility in the structure of (established) materials.

In the context of thin films, structure plays a key role in several applications, such as perfectly conformal layers for electronics applications [18] or protective coatings against corrosion in reactive environments, where grain boundaries might act as diffusion channels and reactive points in crystalline films [19]. It has been shown that the amorphous structure is more resistant to oxidation compared to its polycrystalline counterpart due to the lack of structural order [20,21]. Similarly, grain boundaries together with point defects and surface roughening strongly influence the charge transport properties in the thin-film regime [22]. Understanding and controlling the electrical conductivity at the nanometer scale is for example essential to increase the performance of integrated circuits. In this framework, structural disorder can thus be leveraged to tune the properties of thin films to specific applications.

Among the vast variety of thin-film metallic glasses that have been developed and investigated in literature, CuZr stands out as an ideal system for studying the fundamental role of structure. On the one hand, it is characterized by its excellent glass forming ability [23,24]. On the

other, many crystalline phases and intermetallic compounds are known to form at low temperature [25]. Thus, CuZr is a good model system to study how the thin-film structure affects the material's properties at the atomic scale, with several works reporting an amorphous structure for a wide range of Cu content (18–88 at. %) achieved with sputter-deposition [26,27], co-evaporation [28] and pulsed laser deposition [29].

However, modifying the structure of a metallic thin film without affecting other properties is not straightforward. For instance, the amorphous phase in a binary metal alloy is usually dependent on the stoichiometry of its constituents [30,31]. As mentioned, CuZr is a good example where the compositional range in which the amorphous phase is favoured is particularly large. Other approaches to obtain a glassy structure involve very high cooling rates, which are typically in the order of 10^{14} K s^{-1} for single-element metals [32] and approximately 10^3 K s^{-1} for selected binary alloys [33]. Thus, the deposition of metallic alloys with the same composition but different structure requires dedicated fabrication methods.

In this work, we demonstrate that the level of structural disorder is tunable in thin films of identical composition by tuning the growth parameters of pulsed laser deposition (PLD), allowing for growth far from and close to equilibrium. Adjusting the level of disorder in the layer profoundly impacts the surface chemistry, the electronic transport properties, and the optical transparency of the thin films. Our results establish the essential role that structural disorder plays in the optoelectronic and chemical properties of CuZr thin films. We anticipate the engineering of material properties through structural disorder to be more universally applicable. Such structural tuning opens up a new paradigm in materials design, allowing for the optimization of functional solids for specific technological applications without the need to modify their composition.

2. Results and discussion

To systematically study the impact of disorder on optoelectronic and surface chemical properties of materials, we directly compare CuZr thin films of the same composition with different structure. The exclusive variation of structure is achieved by PLD, which is capable of growing well-defined crystalline as well as off-equilibrium disordered layers. We use the deposition temperature as parameter to vary the level of disorder in the layer, which we probe using grazing-incidence x-ray diffraction (GI-XRD).

Fig. 1(a) shows the results of the structural comparison of CuZr thin films deposited at room temperature (RT, blue curve) and at T ~500 °C (red curve). The diffractograms are fundamentally different. GI-XRD of CuZr grown at RT results in a typical 'liquid-like' pattern expected from a fully amorphous thin film [31,34]. It is characterized by a very broad peak centred at approximately 37.5° with a full-width at half maximum

(FWHM) of 8.5° and a second broad feature at approximately 65.0° with a FWHM of 10.0°. No sharp peaks are present in the GI-XRD pattern. The residual sharp intensity variations above the noise threshold are correlated to the presence of a low density of large crystallites due to melt ejection during deposition. The effect of these droplets on the diffraction results is explained in the supplementary information (Figure S2). On the contrary, the GI-XRD pattern of CuZr thin films deposited at T ~500 °C (red curve in Fig. 1) is characterized by the presence of several sharp peaks attributed to the formation of crystalline grains. The main peaks are located at approximately 33°, 38°, 40°, 44°, 46°, 67° and can be ascribed to different Cu-rich (Cu_8Zr_3 and $Cu_{10}Zr_7$) and Zr-rich ($CuZr_2$) crystal phases [23,26,27], highlighted by triangular, square and circular symbols, respectively. No peaks associated to undesired metal-oxide phases such as ZrO_2 [26,35] were detected. Using the FWHM of the crystalline peaks and the Scherrer equation [36] the mean size of the ordered grains is estimated at approximately 10 nm, which is relatively large compared to the film thickness of this study (~20 nm). The high-temperature deposition of the film within the crystallization temperature range (T_x ~444–527 °C [37,38]) thus allows for sufficient mobility to grow polycrystalline CuZr, consisting of relatively large Cu-rich and Zr-rich grains.

On the other hand, keeping the substrate at RT leads to a rapid quenching of the ablated material in an amorphous structure, which is favoured in the compositional range chosen in this study [23,24]. Annealing the amorphous layer is expected to induce crystallinity at comparable temperatures, but is expected to result in a broader distribution of crystallite sizes and stronger tendency towards break-up and dewetting.

Fig. 1(b) displays an optical photograph of the polycrystalline (top) and the amorphous (bottom) CuZr films, illustrating the dramatic influence of the level of structural disorder on the optical properties of CuZr in the visible spectral range. Despite having the same thickness, the amorphous CuZr thin film is partially transparent, while the polycrystalline layer is opaque, dark and reflective. While these images were acquired in air, the same difference in appearance is also observed immediately after growth in ultra-high vacuum (UHV).

Disorder is also considered a promising parameter to engineer the smoothness and homogeneity of coatings, which we probe using atomic force microscopy (AFM). Indeed, stark differences between the CuZr thin films deposited at RT and at T ~500 °C are observed in the surface topography shown in Fig. 2. The AFM micrograph of the amorphous film deposited at RT shows a smooth, near-featureless morphology down to the nanometer scale. In contrast, the polycrystalline film deposited at T ~500 °C displays a richer morphology dominated by protruding features with a typical diameter of 20–25 nm, comparable to the average thickness of the continuous film. The thin-film surface roughness is significantly lower for the amorphous film than for its polycrystalline
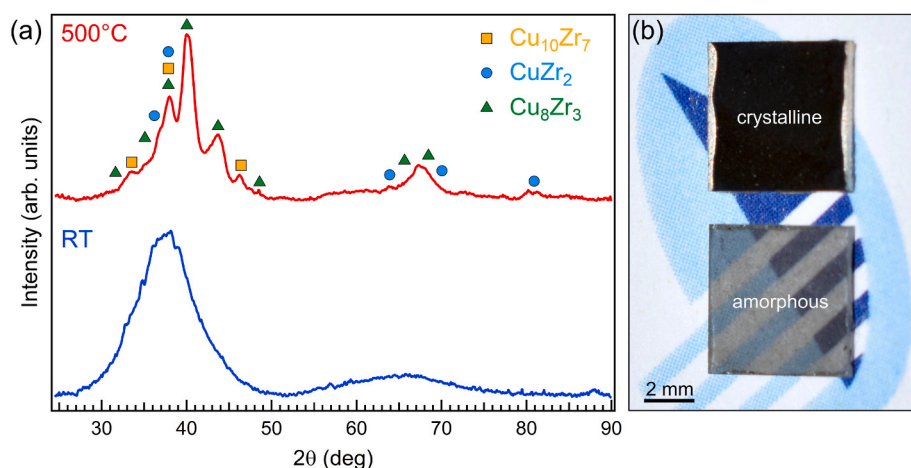

Fig. 1. (a) GI-XRD results of CuZr thin films deposited at room temperature (RT, blue curve) and at 500 °C (red curve). CuZr thin films grown at RT display two very broad, weak peaks, characteristic of an amorphous structure. In contrast, the growth at high temperature favors the formation of a polycrystalline structure of Cu-rich and Zr-rich grains. (b) Photograph of a polycrystalline (top) and amorphous (bottom) CuZr thin film showing stark differences in the visible optical properties: the amorphous film is partially transparent, while the polycrystalline film is opaque and dark.
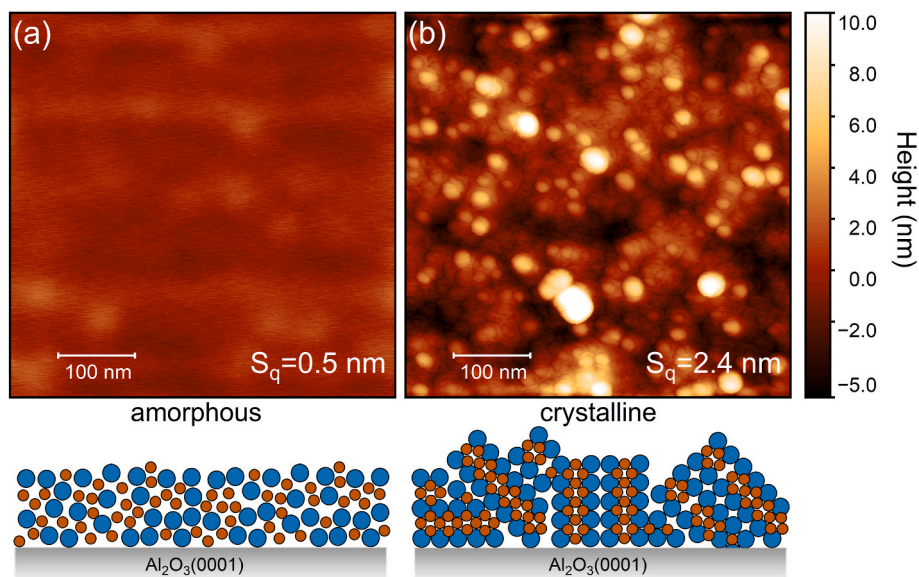
Fig. 2. Atomic force microscopy (AFM) micrographs of an amorphous (a) and a polycrystalline (b) CuZr thin film measured in air. Both images are displayed with the same height scale as indicated by the colour bar. The amorphous film is characterized by a smooth surface with a very low surface roughness, whereas the polycrystalline film presents a grainy surface morphology with a much higher surface roughness, illustrated by the respective schematics below.

counterpart, as quantified by respective root-mean-square height variations S_q of 0.5 nm and 2.4 nm. Such a difference is unsurprising, as the development of grain boundaries in a polycrystalline material is known to promote roughness [31]. Additionally, significant differences in roughness have been previously reported for sputter-deposited CuZr films of various compositions due to composition-induced changes in structure and crystallinity [27,39]. Here, in contrast, the film composition is constant and the difference is thus only due to the

absence/presence of crystallinity.

To study the effect of structural disorder on the surface chemical properties of the CuZr thin films we use x-ray photoelectron spectroscopy (XPS) before and after air exposure. The thin films were first measured in situ after growth in UHV to infer the chemical composition and the purity level of the surface without air exposure. A survey spectrum of an as-grown CuZr thin film is reported in Figure S3(a), showing only core-level peaks ascribed to Cu and Zr, with minor traces
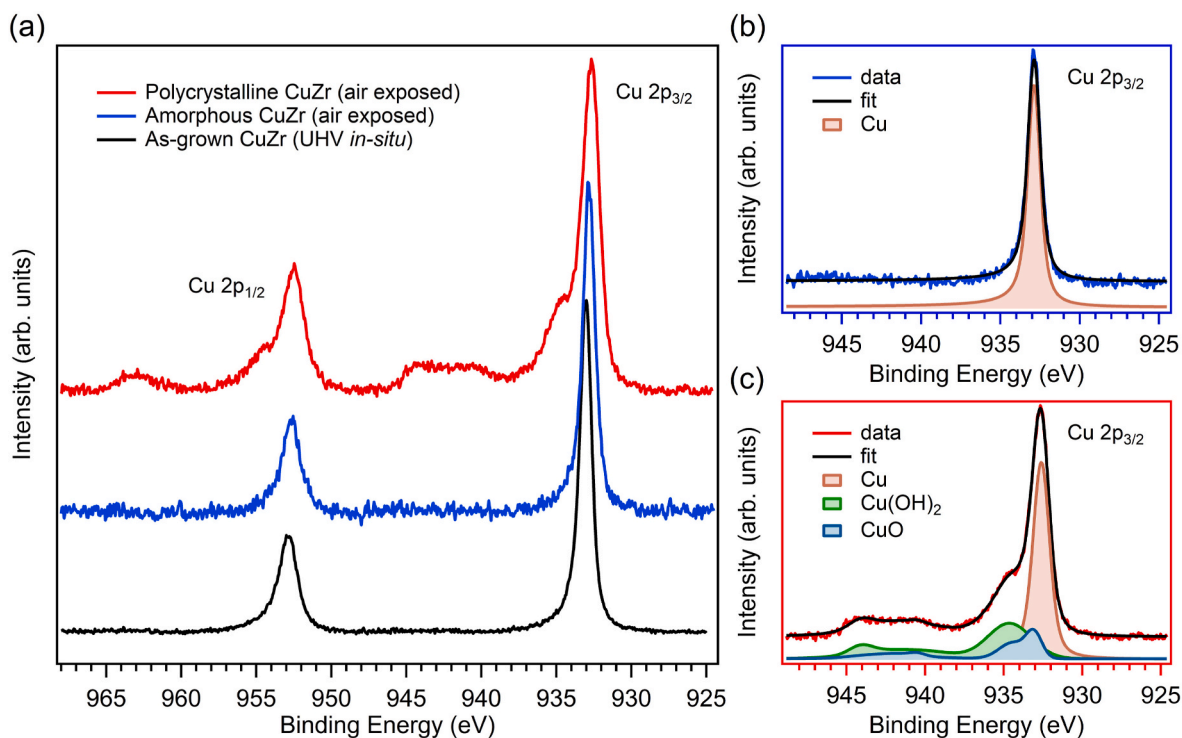

Fig. 3. X-ray photoelectron spectroscopy (XPS) measurements of amorphous vs. crystalline CuZr thin films exposed to air. (a) Cu 2p region of amorphous (blue) and crystalline (red) CuZr thin films after air exposure; the spectrum of an as-grown film (black) acquired in situ is also reported as a comparison. The curves are vertically offset for better visibility. (b) Cu $2p_{3/2}$ region of the amorphous CuZr thin film after air exposure: the spectrum shows a single peak associated with metallic Cu. (c) Cu $2p_{3/2}$ region of the polycrystalline CuZr thin film after air exposure: the spectrum shows three different components associated with metallic Cu, CuO and Cu(OH)$_2$.

of oxygen contamination. The XPS results of amorphous and polycrystalline CuZr thin films after air exposure are reported in Fig. 3. The detailed Cu 2p regions of an amorphous (blue curve) and a polycrystalline (red curve) CuZr thin film exposed to air are compared to an as-grown film (black curve) measured in situ in Fig. 3(a). The Cu 2p spectrum of the air-exposed amorphous film almost exactly matches the spectrum of the as-grown film measured in UHV: the Cu $2p_{3/2}$ peak is fitted with a single component at a binding energy (E_B) of 932.9 eV (Fig. 3(b)), in good agreement with literature values for metallic Cu [40]. No satellite features characteristic of Cu oxide and hydroxide species [40] are detected in the blue and black spectra. To further confirm the assignment as metallic Cu and exclude Cu_2O, the Cu $L_3M_{4,5}M_5$ Auger parameter was calculated, since it has been shown that the Auger spectral line-shape and position directly depends on the Cu oxidation state and species [40,41]. The Cu $L_3M_{4,5}M_5$ Auger spectrum is reported in Figure S4(a): the main peak is located at $E_B = 567.4$ eV, resulting in an Auger parameter $\alpha' = 1851.1$ eV [42], in excellent agreement with the expected value for Cu^0 [40]. These results indicate that Cu is fully metallic both in the as-grown and in the amorphous air-exposed CuZr thin film.

Polycrystalline CuZr, on the other hand, shows a very different Cu 2p XPS spectrum. The red curve in Fig. 3(a) shows the clear presence of a shoulder and a satellite feature at higher binding energy values. The detailed peak-fit reported in Fig. 3(c) reveals the presence of the main metallic Cu $2p_{3/2}$ peak at $E_B = 932.6$ eV together with two sets of components ascribed to CuO and $Cu(OH)_2$ species [40]. The analysis of the corresponding Auger parameters further confirms these results (see Figure S4(b)). These findings indicate that, in contrast to amorphous CuZr thin films, Cu is partially oxidized after air exposure in polycrystalline CuZr.

While air exposure led to very different results regarding the oxidation behavior of Cu in amorphous and polycrystalline CuZr thin films, the behavior of Zr is similar in both cases. Figure S5 reports the detailed XPS spectra of the Zr 3d region for amorphous CuZr (a) and polycrystalline CuZr (b) after air exposure. Both spectra display a main doublet ascribed to ZrO_2 [43], with a Zr $3d_{5/2}$ peak centred at E_B ~182.8 eV. A low-intensity peak at E_B ~179.5 eV ascribed to metallic Zr [43] is visible for the polycrystalline sample, while no other Zr species are detected in the amorphous film. Moreover, the relative surface composition of the films changes dramatically after air exposure, with a reduction of the total Cu XPS intensity and an enrichment of Zr at the surface in both amorphous and polycrystalline CuZr thin films (from XPS we estimate Cu:Zr = 31:69 (±1 at.%) and Cu:Zr = 39:61 (±1 at.%) for amorphous and polycrystalline, respectively).

To identify the difference in oxidation mechanism, the nature of the oxides formed on the amorphous and polycrystalline layers was investigated using Raman spectroscopy measurements in air. Fig. 4 shows the recorded Raman shift for polycrystalline CuZr (red curve), amorphous CuZr (blue curve) and a bare $Al_2O_3(0001)$ substrate (black curve). Again, a clear difference is visible as a function of the thin-film structure. The polycrystalline spectrum is characterized by two very broad but distinct peaks centred at around 277 cm^{-1} and 330 cm^{-1}, which can be ascribed to phonon modes in tetragonal ZrO_2 (t-ZrO_2) and CuO [44,45], respectively, while no clear peaks are detected in the spectrum of the amorphous thin film. Moreover, the characteristic sharp peaks of the sapphire substrate are clearly visible above the background intensity of the amorphous CuZr spectrum, whereas only the most intense peak of the sapphire substrate at approximately 415 cm^{-1} is still detected in the case of polycrystalline CuZr. This strong difference in attenuation is consistent with the observed opaque nature of the polycrystalline layer reported in Fig. 1(b).

The substantial differences in the surface oxidation behavior of air-exposed amorphous and polycrystalline CuZr observed in XPS and Raman spectroscopy allow insights into the structure-dependent oxidation mechanism. As expected for a binary alloy with very different oxygen affinities such as CuZr [21,46], both systems are
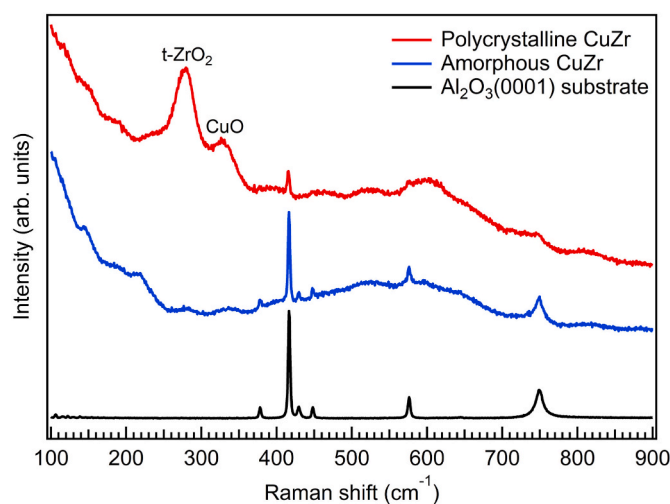
Fig. 4. (a) Ex situ Raman spectroscopy measurements of polycrystalline (red curve) and amorphous (blue curve) CuZr thin films together with a bare $Al_2O_3(0001)$ substrate (black curve), performed with an excitation wavelength of $\lambda = 532$ nm. The curves are vertically offset for better visibility. The spectrum of polycrystalline CuZr is characterized by two broad peaks at 277 cm^{-1} and 330 cm^{-1}, not detected in amorphous CuZr, ascribed to t-ZrO_2 and CuO. The sharp peaks of the $Al_2O_3(0001)$ substrate are still clearly visible above the background in amorphous CuZr, which indicates an overall weak optical absorption of the film around the pump wavelength.

characterized by a strong preferential oxidation and surface enrichment of Zr upon air exposure. However, the structure of the thin film plays a major role. In amorphous CuZr, a ZrO_2 layer fully passivates the surface and prevents Cu underneath from oxidizing. Based on previous reports for air-exposed [47] and thermally oxidized [21] amorphous CuZr films as well as CuZr-based alloys [19], the ZrO_2 layer is expected to be closed and amorphous. The lack of peaks in the Raman spectrum of oxidized amorphous CuZr corroborates this conclusion [48]. The improved oxidation resistance is attributed to the absence of grain boundaries, defined structural defects and energetically favoured interstitial sites that promote O_2 dissolution and diffusion within the film [19–21,49]. Assuming a flat, homogeneous overlayer of amorphous ZrO_2 on crystalline Cu [50], we estimate the thickness of the oxide to be approximately 2.5–3.0 nm.

In polycrystalline CuZr, on the other hand, ZrO_2 is expected to be at least partially crystalline, based on previous findings for thermally oxidized crystalline CuZr [21]. This expectation is confirmed by the observation of peaks ascribed to t-ZrO_2 and CuO in the Raman spectrum. The very large FWHM of these peaks, as compared to the sapphire substrate, indicates the formation of defective oxide crystallites with relatively small grain size, which is also suggested by the lack of corresponding oxide peaks in GI-XRD. The formation of ZrO_2 with a tetragonal structure at RT, instead of the more stable monoclinic one, has already been observed in CuZr thin films for ZrO_2 nanocrystals below a critical size of 30 nm [47]. The rough, polycrystalline CuZr layer thus favours the formation of crystalline oxides and inhibits the formation of a closed amorphous ZrO_2 passivating layer. As a result, grain boundaries and other structural defects are present, which serve as a pathway for O_2 diffusion and act as reactive points. Consequently, Cu is partially oxidized upon air exposure, resulting in an estimated composition of 50% Cu^0, 17% CuO and 33% $Cu(OH)_2$ measured in XPS spectra. The presence of a fraction of Cu_2O in the peak attributed to Cu metal cannot be excluded due to the close overlap of the respective XPS peaks. For Zr, only a small fraction of 5% remains metallic.

The marked difference in the visible optical absorption suggests that the structure might also play a key role in the conductivity of the CuZr thin films. Therefore, we investigate the charge transport properties

from RT down to 4.2 K (liquid He) in a four-probe van der Pauw configuration [51]. Fig. 5 shows the conductivity of polycrystalline (a) and amorphous (b) CuZr thin films as a function of temperature. The conductivity in polycrystalline CuZr is approximately 6.0 mΩ^{-1} cm^{-1} at RT and does not show a clear temperature dependence. Variations in the order of 0.5% are visible and can be ascribed to small modifications in the probe contacts with cooling. In stark contrast, the conductivity of amorphous CuZr is significantly lower, approximately 4.8×10^{-2} mΩ^{-1} cm^{-1} at RT, and decreases with decreasing temperature following an inverse exponential law.

These results clearly indicate that the charge transport follows entirely different mechanisms in amorphous CuZr compared to its polycrystalline counterpart. In general, the conductivity in polycrystalline metallic thin films strongly deviates from the corresponding single-crystalline material and is reduced by point defects, external surfaces and in particular grain boundaries, which are found to be the dominant factor in the thin-film regime [52–54]. The conductivity in polycrystalline CuZr does not show a clear temperature dependence and is approximately two orders of magnitude lower than the value obtained for pure Cu thin films of comparable thickness [55]. This indicates that the characteristic network of grain boundaries strongly reduces the electron mean-free path and dominates the transport properties of the film, which behaves like a defective metal. The temperature-dependent resistivity change of the pure metal thus contributes too little to the overall resistivity to be clearly discernible in the measured temperature range. Similarly, disorder is expected to play a key role in amorphous CuZr, since it increases the electron scattering and reduces the electron mean free path. It is worth noting that the conductivity value at RT in amorphous CuZr is also considerably lower than values reported previously for CuZr [27], and Cu-based [56,57] as well as other amorphous alloys films [58]. This discrepancy might be attributed to size effects based on the film thickness ($\sim$20 nm), which are expected to increase the total resistivity [59].

To understand the temperature-dependence of the conductivity in amorphous CuZr we consider the charge transport mechanism in highly disordered systems, as described in detail by Mott [60]. The conductivity σ in amorphous materials is expected to follow the expression:

$$\sigma(T) = \sigma_0 exp\left(-\frac{T_0}{T}\right)^\alpha$$

where α is a characteristic exponent that assumes the value 1/3 or 1/4 in a two-dimensional and three-dimensional system, respectively. According to this model, known as Mott's variable range hopping conductivity, the theory of conductivity for doped semiconductors can also be applied to amorphous solids. In particular, the absence of long-range order induces a strong localization of the electronic states at individual atomic sites, with no electronic band structure formed in k-space. Similar to conduction in a semiconductor, the charge transport in an amorphous solid is dominated by a thermally activated hopping of electrons between localized states with energies concentrated in a narrow band near the Fermi level [60]. The conductivity is thus strongly dependent on temperature and shows a universal behavior with $\sigma \propto$ exp $(-T_0/T)^\alpha$. The red solid curve in Fig. 5(b) is a fit to Mott's variable range hopping model with $\alpha = 1/4$ (3D), which is found to be in excellent agreement with the experimental data over the entire temperature range (4.2–300 K). This result indicates that the electrons are indeed strongly localized in amorphous CuZr. The observation of three-dimensional hopping conduction indicates that the film thickness ($\sim$20 nm) is significantly larger than the average hopping length, which defines the natural length scale of the process and corresponds to the average separation between available sites [61]. Since the model employed to interpret the transport properties does not provide information about the effective band gap, we derive this property from optical reflectivity measurements (see supplementary information for details). Based on a simple model with a single Lorentzian oscillator, the band gap of amorphous CuZr is estimated at 1.0 ± 0.1 eV, which is in the same range as the gaps of several materials that are heavily used in semiconductor technology.

In addition to the scientific interest in the observed changes in the optical, electronic, and surface chemical properties of CuZr with structural disorder, the additional flexibility of the alloy film with respect to its transparency, corrosion resistance and reactivity, as well as its conductivity and transport mechanism provides an obvious link to a variety of applications. Tuning these properties while maintaining the (metal-based) composition of the layer is attractive in numerous contexts, including metal-based transparent coatings, catalysts with optimized electronic structure, customized corrosion-resistant coatings, and structures with tailored conductivity in the semiconductor industry.

3. Conclusions

In summary, our results demonstrate that the level of structural disorder in alloys is tunable and can induce drastic changes in the electronic, chemical, and optical properties of materials. In a direct comparison of amorphous and crystalline layers grown using PLD, we observe mechanistic differences in oxidation resistance, electronic transport, and optical transparency. The properties of the polycrystalline CuZr layers are dominated by their (defective) crystalline nature including grain boundaries, whereas the disordered nature of amorphous CuZr results in superior corrosion resistance and semiconductor-
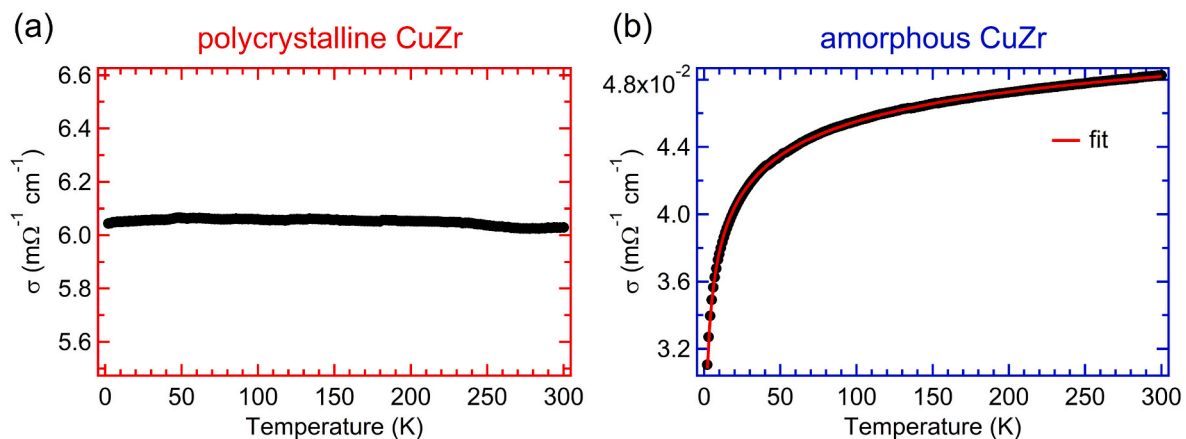

Fig. 5. Conductivity as a function of temperature for polycrystalline (a) and amorphous (b) CuZr thin films measured in a four-probe van der Pauw configuration. The conductivity in polycrystalline CuZr is independent of temperature while in amorphous CuZr it follows an inverse-exponential law as a function of temperature. The red solid curve in (b) is a fit to Mott's variable range hopping 3D model, which is in excellent agreement with the data.

like electronic and optical properties. Our results establish tuning structural disorder in materials as a new route towards customizing functional materials to their application. This approach provides access to new applications for established materials and could loosen rigid constraints on composition in materials design, thus paving the way to the increased use of sustainable materials.

4. Methods

4.1. Sample preparation

CuZr thin films were deposited onto 5×5 mm^2 Al$_2$O$_3$(0001) substrates (Siegert Wafer GmbH) via pulsed laser deposition using a KrF excimer laser ($\lambda = 248$ nm, 20 ns pulse duration) with a typical energy density of 4.5 J/cm^2 and laser repetition rate of 10 Hz. The substrates were cleaned prior to deposition with sequential ultrasonic bath of acetone and isopropanol. A 99.95% pure CuZr (50-50 at.%) target (Alineason Materials Technology GmbH) was used for the deposition process. The base pressure of the system was better than 5.0×10^{-10} mbar. The room temperature depositions were performed in 1.0×10^{-1} mbar Ar (purity 6.0) background pressure. The high-temperature depositions were performed in ultra-high vacuum: an infrared laser heater ($\lambda = 980$ nm) was used to heat the substrates while the temperature was monitored with a pyrometer. The thickness of the thin films was approximately 20 nm, measured with an atomic force microscope. The composition of the deposited thin films was inferred by means of energy-dispersive x-ray spectroscopy (EDX) using a FEI Verios 460 SEM-EDX system equipped with a Schottky field electron gun and an Oxford Xmax 80 detector. The measured composition was found to be CuZr: 44–56 ± 1 at.% for room temperature depositions and CuZr: 43–57 ± 1 at.% for high-temperature depositions (T ~500 °C). The difference between film and target composition, i.e. the slight enrichment in total Zr content of the film, can be ascribed to resputtering effects typical of metals and alloys deposited with pulsed laser deposition [62,63].

4.2. X-ray diffraction

The structural properties of CuZr thin films were investigated ex situ by means of x-ray diffraction measurements in grazing-incidence configuration to minimize the contribution of the substrate. The GI-XRD investigation was performed using a Bruker D8 QUEST diffractometer system equipped with an Incoatec IμS 3.0 CuKα x-ray source ($\lambda = 1.5406$ Å) and a PHOTON II Charge-integrating Pixel Array Detector (CPAD). Outliers corresponding to isolated saturated pixels of the detector have been removed in Fig. 1(a). The raw data are shown in Figure S1 of the supplementary information.

4.3. Atomic force microscopy

AFM measurements were performed using a Bruker Dimension Icon system operated in tapping mode. The measurements were carried out inside a soundproof chamber on a vibration isolation table. The images were processed and analysed using Gwyddion software.

4.4. X-ray photoelectron spectroscopy

XPS measurements were performed in a UHV setup (base pressure better than 1.0×10^{-9} mbar) equipped with a Scienta Omicron R4000 HiPP-3 analyser (swift acceleration mode, 1 mm entrance slit) and a monochromatic Al-Kα x-ray source (1486.6 eV). The CuZr thin films were first investigated in situ to infer the chemical composition of the surface: the samples were transferred from the PLD growth chamber to the XPS analysis chamber via an UHV transfer system to prevent contamination due to air exposure. The ex situ measurements (i.e. after air exposure) were performed on samples kept in the same ambient conditions for approximately two weeks. Survey spectra were recorded at a pass energy (PE) of 500 eV, while detailed spectra were recorded at PE = 100 eV. The spectra were processed and analysed using KolXPD software (Kolibrik).

4.5. Optical spectroscopy

A WITec alpha300 confocal Raman microscope was used to perform Raman spectroscopy measurements ex situ on CuZr thin films. The samples were mounted on a capacitive controlled piezo-stage with 3 nm lateral positioning accuracy. A continuous laser ($\lambda = 532$ nm) was used as excitation wavelength and focused on the sample by a Zeiss EC Epiplan-Neofluar 100x objective (NA = 0.9). The scattered light was collected by the same objective and detected with a fibre-coupled WITec UHTS 300 spectrometer (blaze wavelength 500 nm and 600 g/mm grating) and an Andor EMCCD. Fourier transform infrared spectroscopy was used to determine the reflectivity of the samples over the energy range from 4 meV to 2.7 eV using a previously reported combination of sources, beam-splitters and detectors [64].

4.6. Transport measurements

Resistance measurements were carried out in the temperature range 4.2–300 K in a Physical Properties Measurement System/Dynacool (Quantum Design) using the resistivity option. Current and voltage contacts were attached to the corners of the samples by silver paint. Resistance data were taken in two van der Pauw configurations, after which the conductivity $\sigma(T)$ was evaluated by the van der Pauw relation [51]. The excitation current was 1 μA.

Credit author statement

Alessandro Troglia: Investigation, Visualization, Methodology, Writing- Original Draft (Introduction, Results, Discussion and Methods), **Victor Vollema:** Investigation (Atomic Force Microscopy), Methodology, **Silvia Cassanelli:** Investigation (Reflectivity) **Erik van Heumen:** Investigation (Reflectivity), Writing (Reflectivity), Supervision (Reflectivity), **Jorik van de Groep:** Investigation (Raman), Writing (Raman), Writing- Review & Editing, **Anne de Visser:** Investigation (Transport Measurements), Writing (Transport), Methodology, **Roland Bliem:** Supervision, Writing – Original Draft (Abstract, Introduction), Writing – Review & Editing, Project Administration.

Declaration of competing interest

The authors declare that they have no known competing financial interests or personal relationships that could have appeared to influence the work reported in this paper.

Data availability

Data will be made available on request.

Acknowledgments

Appendix A. Supplementary data

Supplementary data to this article can be found online at https://doi.org/10.1016/j.mtphys.2022.100893.

References

[1] C.J. Byrne, M. Eldrup, Bulk metallic glasses, Science 321 (2008) 502–503, https://doi.org/10.1126/science.1158864.

[2] W.H. Wang, Bulk metallic glasses with functional physical properties, Adv. Mater. 21 (2009) 4524–4544, https://doi.org/10.1002/adma.200901053.

[3] A. Greer, Metallic glasses, in: D.E. Laughlin, K. Hono (Eds.), Physical Metallurgy, fifth ed., Elsevier, Oxford, 2014, pp. 305–385, https://doi.org/10.1016/B978-0-444-53770-6.00004-6, fifth edition Edition.

[4] Q. Halim, N.A.N. Mohamed, M.R.M. Rejab, W.N.W.A. Naim, Q. Ma, Metallic glass properties, processing method and development perspective: a review, Int. J. Adv. Manuf. Technol. 112 (2021) 1231–1258, https://doi.org/10.1007/s00170-020-06515-z.

[5] K. Asami, K. Hashimoto, T. Masumoto, S. Shimodaira, Esca study of the passive film on an extremely corrosion-resistant amorphous iron alloy, Corrosion Sci. 16 (1976) 909–914, https://doi.org/10.1016/S0010-938X(76)80010-8.

[6] J.R. Scully, A. Gebert, J.H. Payer, Corrosion and related mechanical properties of bulk metallic glasses, J. Mater. Res. 22 (2007) 302–313, https://doi.org/10.1557/jmr.2007.0051.

[7] H.S. Chen, Glassy metals, Rep. Prog. Phys. 43 (1980) 353–432, https://doi.org/10.1088/0034-4885/43/4/001.

[8] J.J. Gilman, Metallic glasses, Science 208 (1980) 856–861, https://doi.org/10.1126/science.208.4446.856.

[9] M. Ishida, H. Takeda, N. Nishiyama, K. Kita, Y. Shimizu, Y. Saotome, A. Inoue, Wear resistivity of super-precision microgear made of Ni-based metallic glass, Mater. Sci. Eng., A 449–451 (2007) 149–154, https://doi.org/10.1016/j.msea.2006.02.300.

[10] J.C. Barbour, F.W. Saris, M. Nastasi, J.W. Mayer, Amorphous ni-zr alloys as barriers for self-diffusion, Phys. Rev. B 32 (1985) 1363–1365, https://doi.org/10.1103/PhysRevB.32.1363.

[11] D.L. Cocke, Heterogeneous catalysis by amorphous materials, J. Met. 10 (1986) 70–74, https://doi.org/10.1016/0079-6786(75)90006-0.

[12] B.R. Goldsmith, B. Peters, J.K. Johnson, B.C. Gates, S.L. Scott, Beyond ordered materials: understanding catalytic sites on amorphous solids, ACS Catal. 7 (2017) 7543–7557, https://doi.org/10.1021/acscatal.7b01767.

[13] M.M. Trexler, N.N. Thadhani, Mechanical properties of bulk metallic glasses, Prog. Mater. Sci. 55 (2010) 759–839, https://doi.org/10.1016/j.pmatsci.2010.04.002.

[14] O. Hunderi, Optical properties of disordered and amorphous metal films, Thin Solid Films 37 (1976) 275–280, https://doi.org/10.1016/0040-6090(76)90194-2.

[15] Z.H. Stachurski, On structure and properties of amorphous materials, Materials 4 (2011) 1564–1598, https://doi.org/10.3390/ma4091564.

[16] J.P. Chu, J. Jang, J. Huang, H. Chou, Y. Yang, J. Ye, Y. Wang, J. Lee, F. Liu, P. Liaw, Y. Chen, C. Lee, C. Li, C. Rullyani, Thin film metallic glasses: unique properties and potential applications, Thin Solid Films 520 (2012) 5097–5122, https://doi.org/10.1016/j.tsf.2012.03.092.

[17] P. Yiu, W. Diyatmika, N. Bönninghoff, Y.-C. Lu, B.-Z. Lai, J.P. Chu, Thin film metallic glasses: properties, applications and future, J. Appl. Phys. 127 (2020): 030901, https://doi.org/10.1063/1.5122884.

[18] R.W. Johnson, A. Hultqvist, S.F. Bent, A brief review of atomic layer deposition: from fundamentals to applications, Mater. Today 17 (2014) 236–246, https://doi.org/10.1016/j.mattod.2014.04.026.

[19] Y. Xu, L. Jeurgens, L. Lin, S. Ma, S. Zhu, Y. Huang, Y. Liu, J. Qiao, Z. Wang, Revealing the univariate effect of structural order on the oxidation of ternary alloys: amorphous vs. crystalline Cu–Zr–Al alloys, Corrosion Sci. 183 (2021): 109309, https://doi.org/10.1016/j.corsci.2021.109309.

[20] K.R. Lim, J.M. Park, S.J. Kim, E.-S. Lee, W.T. Kim, A. Gebert, J. Eckert, D.H. Kim, Enhancement of oxidation resistance of the supercooled liquid in Cu–Zr-based metallic glass by forming an amorphous oxide layer with high thermal stability, Corrosion Sci. 66 (2013) 1–4, https://doi.org/10.1016/j.corsci.2012.09.018.

[21] Y. Xu, L.P. Jeurgens, P. Schützendübe, S. Zhu, Y. Huang, Y. Liu, Z. Wang, Effect of atomic structure on preferential oxidation of alloys: amorphous versus crystalline Cu-Zr, J. Mater. Sci. Technol. 40 (2020) 128–134, https://doi.org/10.1016/j.jmst.2019.10.001.

[22] R.C. Munoz, C. Arenas, Size effects and charge transport in metals: quantum theory of the resistivity of nanometric metallic structures arising from electron scattering by grain boundaries and by rough surfaces, Appl. Phys. Rev. 4 (2017): 011102, https://doi.org/10.1063/1.4974032.

[23] O.J. Kwon, Y.C. Kim, K.B. Kim, Y.K. Lee, E. Fleury, Formation of amorphous phase in the binary Cu-Zr alloy system, Met. Mater. Int. 12 (2006) 207–212, https://doi.org/10.1007/BF03027532.

[24] Z.-Y. Wei, C. Shang, X.-J. Zhang, Z.-P. Liu, Glassy nature and glass-to-crystal transition in the binary metallic glass CuZr, Phys. Rev. B 95 (2017): 214111, https://doi.org/10.1103/PhysRevB.95.214111.

[25] H. Okamoto, Cu-Zr (copper-zirconium), J. Phase Equilibria Diffus. 33 (2012) 417–418, https://doi.org/10.1007/s11669-012-0077-1.

[26] M. Apreutesei, P. Steyer, L. Joly-Pottuz, A. Billard, J. Qiao, S. Cardinal, F. Sanchette, J. Pelletier, C. Esnouf, Microstructural, thermal and mechanical behavior of co-sputtered binary Zr–Cu thin film metallic glasses, Thin Solid Films 561 (2014) 53–59, https://doi.org/10.1016/j.tsf.2013.05.177, properties and Applications of Thin Film Metallic Glasses.

[27] P. Zeman, M. Zítek, Š. Zuzjaková, R. Čerstvý, Amorphous Zr-Cu thin-film alloys with metallic glass behavior, J. Alloys Compd. 696 (2017) 1298–1306, https://doi.org/10.1016/j.jallcom.2016.12.098.

[28] T. Minemura, J.J. van den Broek, J.L.C. Daams, Formation and thermal stability of amorphous Cu-Zr thin films deposited by coevaporation, J. Appl. Phys. 63 (1988) 4426–4430, https://doi.org/10.1063/1.340188.

[29] G.A. Almyras, G.M. Matenoglou, P. Komninou, C. Kosmidis, P. Patsalas, G. A. Evangelakis, On the deposition mechanisms and the formation of glassy CU–Zr thin films, J. Appl. Phys. 107 (2010): 084313, https://doi.org/10.1063/1.3366715.

[30] W.L. Johnson, Bulk glass-forming metallic alloys: science and technology, MRS Bull. 24 (1999) 42–56, https://doi.org/10.1557/proc-554-311.

[31] G. Yetik, A. Troglia, S. Farokhipoor, S. van Vliet, J. Momand, B.J. Kooi, R. Bliem, J. W. Frenken, Ultrathin, sputter-deposited, amorphous alloy films of ruthenium and molybdenum, Surf. Coating. Technol. 445 (2022): 128729, https://doi.org/10.1016/j.surfcoat.2022.128729.

[32] L. Zhong, J. Wang, H. Sheng, Z. Zhang, S.X. Mao, Formation of monatomic metallic glasses through ultrafast liquid quenching, Nature 512 (2014) 177–180, https://doi.org/10.1038/nature13617.

[33] W.H. Wang, Roles of minor additions in formation and properties of bulk metallic glasses, Prog. Mater. Sci. 52 (2007) 540–596, https://doi.org/10.1016/j.pmatsci.2006.07.003.

[34] B. Braeckman, D. Depla, On the amorphous nature of sputtered thin film alloys, Acta Mater. 109 (2016) 323–329, https://doi.org/10.1016/j.actamat.2016.02.035.

[35] M. Ghidelli, A. Orekhov, A.L. Bassi, G. Terraneo, P. Djemia, G. Abadias, M. Nord, A. Béché, N. Gauquelin, J. Verbeeck, J.-P. Raskin, D. Schryvers, T. Pardoen, H. Idrissi, Novel class of nanostructured metallic glass films with superior and tunable mechanical properties, Acta Mater. 213 (2021): 116955, https://doi.org/10.1016/j.actamat.2021.116955.

[36] B. Cullity, S. Stock, Elements of X-Ray Diffraction, third ed., Prentice-Hall, 2001.

[37] P. Yu, H. Bai, M. Tang, W. Wang, Excellent glass-forming ability in simple $Cu_{50}Zr_{50}$-based alloys, J. Non-Cryst. Solids 351 (2005) 1328–1332, https://doi.org/10.1016/j.jnoncrysol.2005.03.012.

[38] D. Lee, B. Zhao, E. Perim, H. Zhang, P. Gong, Y. Gao, Y. Liu, C. Toher, S. Curtarolo, J. Schroers, J.J. Vlassak, Crystallization behavior upon heating and cooling in $Cu_{50}Zr_{50}$ metallic glass thin films, Acta Mater. 121 (2016) 68–77, https://doi.org/10.1016/j.actamat.2016.08.076.

[39] A. Rauf, C. Guo, Y. Fang, Z. Yu, B. Sun, T. Feng, Binary Cu-Zr thin film metallic glasses with tunable nanoscale structures and properties, J. Non-Cryst. Solids 498 (2018) 95–102, https://doi.org/10.1016/j.jnoncrysol.2018.06.015.

[40] M.C. Biesinger, Advanced analysis of copper x-ray photoelectron spectra, Surf. Interface Anal. 49 (2017) 1325–1334, https://doi.org/10.1002/sia.6239.

[41] S. Saikova, S. Vorobyev, M. Likhatski, A. Romanchenko, S. Erenburg, S. Trubina, Y. Mikhlin, X-ray photoelectron, Cu L_3MM auger and x-ray absorption spectroscopic studies of Cu nanoparticles produced in aqueous solutions: the effect of sample preparation techniques, Appl. Surf. Sci. 258 (2012) 8214–8221, https://doi.org/10.1016/j.apsusc.2012.05.024.

[42] S.W. Gaarenstroom, N. Winograd, Initial and final state effects in the esca spectra of cadmium and silver oxides, J. Chem. Phys. 67 (1977) 3500–3506, https://doi.org/10.1063/1.435347.

[43] I. Bespalov, M. Datler, S. Buhr, W. Drachsel, G. Rupprechter, Y. Suchorski, Initial stages of oxide formation on the zr surface at low oxygen pressure: an in situ fim and xps study, Ultramicroscopy 159 (2015) 147–151, https://doi.org/10.1016/j.ultramic.2015.02.016.

[44] S. N. Basahel, M. Mokhtar, E. H. Alsharaeh, T. T. Ali, H. A. Mahmoud, K. Narasimharao, Physico-chemical and catalytic properties of mesoporous CuO-Zro$_2$ catalysts, Catalysts 6. doi:https://doi.org/10.3390/catal6040057.

[45] J.F. Xu, W. Ji, Z.X. Shen, W.S. Li, S.H. Tang, X.R. Ye, D.Z. Jia, X.Q. Xin, Raman spectra of CuO nanocrystals, J. Raman Spectrosc. 30 (1999) 413–415, https://doi.org/10.1002/(SICI)1097-4555(199905)30:5<413::AID-JRS387>3.0.CO;2-N.

[46] X. Li, J. Wu, J. Pan, Preparation of nanostructured Cu/Zr metal mixed oxides via self-sustained oxidation of a CuZr binary amorphous alloy, J. Mater. Sci. Technol. 35 (2019) 1601–1606, https://doi.org/10.1016/j.jmst.2019.03.020.

[47] Y. Xu, X. Liu, L. Gu, J. Wang, P. Schützendübe, Y. Huang, Y. Liu, Z. Wang, Natural oxidation of amorphous Cu_xZr_{1-x} alloys, Appl. Surf. Sci. 457 (2018) 396–402, https://doi.org/10.1016/j.apsusc.2018.06.130.

[48] D.S.S. Padovini, D.S.L. Pontes, C.J. Dalmaschio, F.M. Pontes, E. Longo, Facile synthesis and characterization of ZrO_2 nanoparticles prepared by the AOP/hydrothermal route, RSC Adv. 4 (2014) 38484–38490, https://doi.org/10.1039/C4RA04861J.

[49] M. Kotrlová, P. Zeman, Š. Zuzjaková, M. Zítek, On crystallization and oxidation behavior of $Zr_{54}Cu_{46}$ and $Zr_{27}Hf_{27}Cu_{46}$ thin-film metallic glasses compared to a crystalline $Zr_{54}Cu_{46}$ thin-film alloy, J. Non-Cryst. Solids 500 (2018) 475–481, https://doi.org/10.1016/j.jnoncrysol.2018.09.004.

[50] A. Jablonski, J. Zemek, Overlayer thickness determination by xps using the multiline approach, Surf. Interface Anal. 41 (3) (2009) 193–204, https://doi.org/10.1002/sia.3005.

[51] L.J. van der Pauw, A method of measuring specific resisitivity and Hall effect of discs of arbitrary shape, Philips Res. Rep. 13 (1958) 1–9.

[52] A.F. Mayadas, M. Shatzkes, Electrical-resistivity model for polycrystalline films: the case of arbitrary reflection at external surfaces, Phys. Rev. B 1 (1970) 1382–1389, https://doi.org/10.1103/PhysRevB.1.1382.

[53] G. Reiss, J. Vancea, H. Hoffmann, Grain-boundary resistance in polycrystalline metals, Phys. Rev. Lett. 56 (1986) 2100–2103, https://doi.org/10.1103/PhysRevLett.56.2100.

[54] L. Moraga, C. Arenas, R. Henriquez, S. Bravo, B. Solis, The electrical conductivity of polycrystalline metallic films, Phys. B Condens. Matter 499 (2016) 17–23, https://doi.org/10.1016/j.physb.2016.07.001.

[55] F. Cemin, D. Lundin, D. Cammilleri, T. Maroutian, P. Lecoeur, T. Minea, Low electrical resistivity in thin and ultrathin copper layers grown by high power impulse magnetron sputtering, J. Vac. Sci. Technol. 34 (2016): 051506, https://doi.org/10.1116/1.4959555.

[56] Y.K. Kuo, K.M. Sivakumar, C.A. Su, C.N. Ku, S.T. Lin, A.B. Kaiser, J.B. Qiang, Q. Wang, C. Dong, Measurement of low-temperature transport properties of Cu-based Cu-Zr-Ti bulk metallic glass, Phys. Rev. B 74 (2006): 014208, https://doi.org/10.1103/PhysRevB.74.014208.

[57] H. Turnow, H. Wendrock, S. Menzel, T. Gemming, J. Eckert, Structure and properties of sputter deposited crystalline and amorphous Cu–Ti films, Thin Solid Films 598 (2016) 184–188, https://doi.org/10.1016/j.tsf.2015.10.081.

[58] D. You, H. Zhang, S. Ganorkar, T. Kim, J. Schroers, J.J. Vlassak, D. Lee, Electrical resistivity as a descriptor for classification of amorphous versus crystalline phases of alloys, Acta Mater. 231 (2022): 117861, https://doi.org/10.1016/j.actamat.2022.117861.

[59] G. Palasantzas, Y.-P. Zhao, G.-C. Wang, T.-M. Lu, J. Barnas, J.T.M. De Hosson, Electrical conductivity and thin-film growth dynamics, Phys. Rev. B 61 (2000) 11109–11117, https://doi.org/10.1103/PhysRevB.61.11109.

[60] N.F. Mott, Conduction in non-crystalline materials, Phil. Mag. 19 (1969) 835–852.

[61] B.I. Shklovskii, A.L. Efros, Electronic Properties of Doped Semiconductors, first ed., Springer Berlin, Heidelberg, 1984 https://doi.org/10.1007/978-3-662-02403-4.

[62] S. Fähler, K. Sturm, H.-U. Krebs, Resputtering during the growth of pulsed-laser-deposited metallic films in vacuum and in an ambient gas, Appl. Phys. Lett. 75 (1999) 3766–3768, https://doi.org/10.1063/1.125449.

[63] K. Sturm, S. Fähler, H.-U. Krebs, Pulsed laser deposition of metals in low pressure inert gas, Appl. Surf. Sci. 154–155 (2000) 462–466, https://doi.org/10.1016/S0169-4332(99)00407-9.

[64] A. Tytarenko, Exploring Instabilities of Bad Metals with Optical Spectroscopy, Ph.D. thesis, University of Amsterdam, 2017.